PHYSICAL REVIEW C **92**, 011602(R) (2015)

Superfluid dynamics of ^{258}Fm fission

Guillaume Scamps*
GANIL, CEA/DSM, and CNRS/IN2P3, Boîte Postale 55027, 14076 Caen Cedex, France, and Department of Physics, Tohoku University, Sendai 980-8578, Japan

Cédric Simenel†
Department of Nuclear Physics, Research School of Physics and Engineering Australian National University, Canberra, Australian Capital Territory 2601, Australia

Denis Lacroix‡
Institut de Physique Nucléaire, IN2P3-CNRS, Université Paris-Sud, F-91406 Orsay Cedex, France

(Received 15 January 2015; revised manuscript received 28 April 2015; published 23 July 2015)

The theoretical description of nuclear fission remains one of the major challenges of quantum many-body dynamics. The motion through the fission barrier is followed by a fast, nonadiabatic descent of the potential between the fragments. The latter stage is crucial as it generates most of the excitation energy in the fragments. The superfluid dynamics in the latter stage of fission is obtained from the time-dependent Hartree-Fock theory including BCS dynamical pairing correlations. The fission modes of the ^{258}Fm nucleus are studied. The resulting fission fragment characteristics show good agreement with experimental data. Quantum shell effects are shown to play a crucial role in the dynamics and formation of the fragments. The importance of quantum fluctuations beyond the independent particle and quasiparticle picture is emphasized and qualitatively studied.

DOI: 10.1103/PhysRevC.92.011602 PACS number(s): 24.75.+i, 21.60.Jz, 27.90.+b

Since its discovery in 1939 [1,2], the fission process has been a pillar of nuclear physics as well as atomic cluster studies [3]. It is the process revealing most clearly the complexity of low-energy nuclear dynamics. Thus, it provides an ideal test for the modeling of nuclear systems with quantum many-body theories. It has also found important applications in fundamental science. For instance, it is the best way to produce beams of exotic rare isotopes in present and future accelerators. In addition, understanding fission dynamics is crucial for the production of superheavy elements, an important motivation for the construction of exotic beam accelerators. Fission is also present in some astrophysical processes. In fact, the natural abundance of elements heavier than iron is believed to be largely influenced by the fission of very neutron-rich heavy nuclei formed in supernovae and neutron star mergers [4]. Moreover, nuclear fission is one of the greatest sources of energy available on Earth. Safely extracting this energy to produce electricity while preserving our environment has been, and still is, one of the greatest technological challenges of humanity.

The theoretical description of the nuclear fission phenomenon remains a profound problem in fundamental science. In order for fission to occur, nuclei have to overcome the fission barrier, which involves dissipative motion. This process has been widely modeled using the adiabatic approximation [5]. This approximation is justified when the evolution of the collective coordinate is slow enough to allow the internal degrees of freedom to be equilibrated. However, close to the scission, an acceleration of the fragments occurs, inducing nonadiabatic effects. Thus, the adiabatic approximation breaks down in the latter stage of fission, where the evolution is faster. In particular, the dynamics near scission, where the fragments separate, is clearly nonadiabatic [6,7]. These effects are crucial to properly describe properties of the fragments such as their mass, charge, and their excitation energy. In particular, the latter determines the number of emitted neutrons and is thus one of the most important properties for the simulation and safety of future nuclear reactors.

The complexity of fission dynamics and the high number of degrees of freedom to be included motivate the use of microscopic approaches, where the quantum behavior of each and every nucleon in the whole system is followed in time. Microscopic approaches have recently considerably improved our understanding of the fission process [7–20]. Time dependence is also a key to addressing the latter stage of the fission process [19,21,22]. Nonadiabatic effects in the latter stage of fission have recently been investigated in fission of ^{264}Fm using a time-dependent mean-field approach [19]. As an example of new outcomes, it was shown that more than half of the final excitation energy of the fragments is acquired during the last zeptosecond before scission and that it is at least partly stored in low-energy collective vibrational states of the fragments. However, the calculations in Ref. [19] are based on an independent particle approximation and pairing correlations responsible for a superfluid phase in nuclear systems were neglected, thus limiting the range of possible applications to few nonsuperfluid systems. It is then crucial to incorporate time-dependent pairing correlations in order to investigate fission dynamics across the nuclear chart. These correlations have been recently included in realistic time-dependent mean-field calculations [23–27], which we extend to the study of fission.

*scamps@nucl.phys.tohoku.ac.jp
†cedric.simenel@anu.edu.au
‡lacroix@ipno.in2p3.fr

The purpose of this Rapid Communication is to present a microscopic method which incorporates both superfluid dynamics and nonadiabatic effects in the latter stage of the fission process. Fission in the ^{258}Fm nucleus is considered as an example of application. This nucleus is known experimentally to exhibit bimodal fission [28] and constitutes an ideal benchmark for theoretical studies of fission [7,9,10,29,30].

In the present approach, it is assumed that the fission process is divided into two steps. In the first step, the slow evolution near the fission barrier is treated in a standard way using the adiabatic approximation. The constrained Hartree-Fock (HF) equations with pairing correlations are solved at the BCS level (CHF+BCS). Several constraints are considered in order to find different valleys in the potential energy surface. In the second step, the descent of the potential towards scission is determined using the time-dependent HF equations with dynamical pairing correlations (TDBCS). The properties of the fragments, in particular their mass, charge, and kinetic energy, are then computed after scission and compared with experimental data from Ref. [28].

The mean field is obtained with the Sly4d [31] Skyrme energy density functional and a constant-G interaction in the pairing channel. The pairing strength is chosen to be $G_n = 24/N$ MeV and $G_p = 19/Z$ MeV. Density-dependent pairing interactions have also been tested and lead to similar results. The CHF+BCS and TDBCS calculations are obtained with modified versions of the EV8 [32] and TDHF3D [31] codes, respectively, assuming only one plane of symmetry. Spatial symmetries of the initial state are preserved in the mean-field dynamics, whether or not the numerical code includes explicitly such symmetries. Time-odd terms are also included, which is crucial for a proper description of dissipation [33,34]. All calculations are performed on a Cartesian grid of $88 \times 19.2 \times 19.2$ fm^3 with a mesh size of 0.8 fm. The time evolution is obtained with a time step of 1.5×10^{-24} s.

The CHF+BCS solutions with constraints on quadrupole Q_{20}, octupole Q_{30}, and hexadecapole Q_{40} moments along the fission axis let appear three valleys. Two valleys with a total $Q_{30} = 0$ lead to symmetric compact fragments (scf) and to symmetric elongated fragments (sef), respectively. In the scf valley, the final fragments are almost spherical while they exhibit a strong prolate shape in the sef valley. A third valley with $Q_{30} \neq 0$ leads to asymmetric elongated fragments (aef) with different masses and charges. Similar adiabatic valleys were obtained by other groups for the same nucleus [9,10,30]. The potential energy along these three valleys is shown in Fig. 1.

Let us now investigate the second stage of the fission process, associated with the descent of the potential towards scission. TDBCS calculations have been performed with initial configurations along those valleys indicated by arrows in Fig. 1. These initial configurations are chosen such that varying the initial Q_{20} by ∼40 b does not affect the final properties of the fragments. This lack of sensitivity with the initial condition indicates that the early stages of the TDBCS evolution are indeed mostly adiabatic while the nonadiabatic effects appear closer to scission. Ideally, one would like to start the dynamical calculations as close as possible to the fission barrier to reach

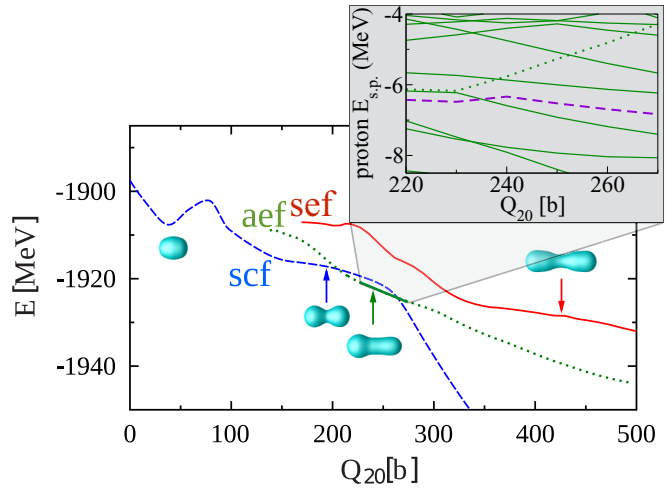

FIG. 1. (Color online) Potential energy in the three valleys: symmetric compact fragment (scf) (dashed blue [gray] line), symmetric elongated fragment (sef) (solid red [gray] line), and asymmetric elongated fragment (aef) (dotted green [gray] line). The arrows correspond to the starting configurations of the dynamical calculations for each mode. Isodensities at half the saturation density $\rho_0/2 = 0.08$ fm^{-3} are also plotted at these initial configurations and for the ^{258}Fm ground state (left). The inset shows the adiabatic single-proton energies $E_{s.p.}$ for the aef mode near the starting configuration where a single-particle level (dotted line) leaves the Fermi surface (dashed line).

a dynamical description of most of the potential descent. However, residual interaction beyond the independent particle or quasiparticle theory would be required to describe the evolution near the barrier [22].

Nevertheless, the present choices of initial configurations are able to capture the transition from adiabatic to nonadiabatic evolution.

The density evolutions in the dynamical phase are represented at various times for each mode in Fig. 2. The asymmetric mode is likely to be responsible for the tail of the experimental fragment mass distribution shown in the inset of Fig. 3. It is also interesting to note that the three evolutions require different times to reach scission. These times are ∼2, ∼5.4, and ∼3.2 zs for the scf, aef, and sef modes, respectively.

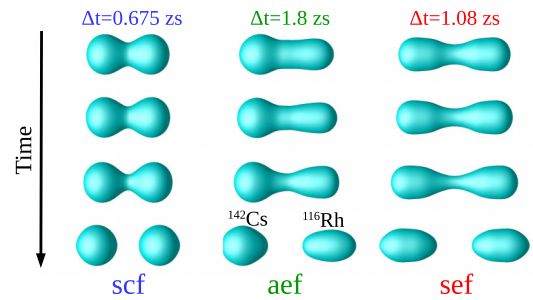

FIG. 2. (Color online) Isodensity surfaces at half the saturation density $\rho_0/2 = 0.08$ fm^{-3} as a function of time for the three modes. The time steps between two images Δt are given at the top of the figure.

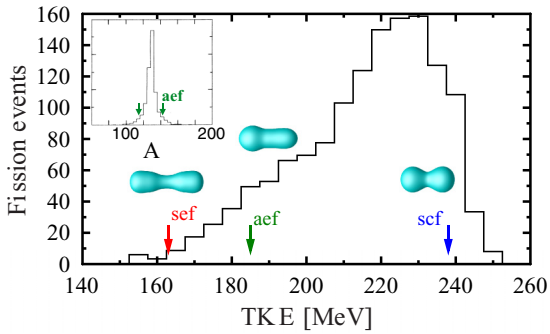

FIG. 3. (Color online) Experimental distribution of TKE from Ref. [28]. The arrows correspond to the TDBCS prediction of the mean value of the TKE. The fragment mass distribution is shown in the inset.

These variations are likely to be due to a combination of two factors: different potential slopes and different one-body viscosity, which is expected to depend on shell effects. Pairing dynamics may also strongly affect the evolution. The TDBCS approach takes into account changes in occupation numbers when single-particle levels cross the Fermi surface, leading to variations in pairing energy as shown in Fig. 4(a) for the aef mode. We also see in Fig. 4(b) that dynamical pairing favors fission as the fragments separate faster in TDBCS than in the frozen occupation approximation (FOA). TDBCS calculations can then start from more compact configurations where single-particle levels still cross the Fermi surface and yet lead to fission. This is illustrated in the inset of Fig. 1 showing, as an example, the evolution of adiabatic proton single-particle energies in the aef mode. The level represented with a dotted line initially lies just above the Fermi level, but close enough to have a significant occupation number greater than 0.4 until it leaves the the Fermi surface at 240 b, where it rapidly drops. This level is responsible for the FOA trajectory not being able

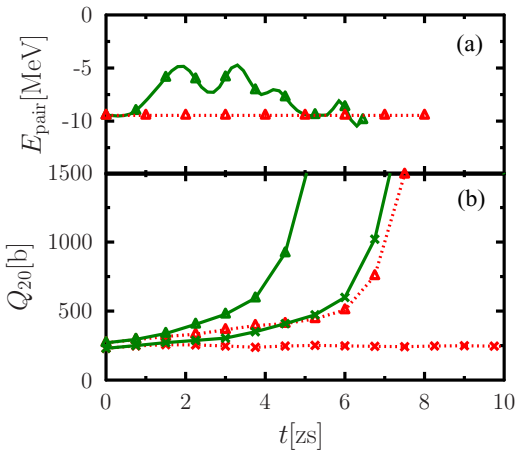

FIG. 4. (Color online) Comparison of time evolution of (a) pairing energy and (b) quadrupole moment obtained with TDBCS (solid lines) and with FOA (dotted lines) for the aef mode. Two initial deformations $Q_{20} = 230$ b (crosses) and $Q_{20} = 270$ b (triangles) are compared in panel (b).

to fission when starting with smaller Q_{20} [see Fig. 2(b)] as the FOA keeps the initial occupation number of this state constant while it should go to zero, leading to a spurious increase of the potential energy between the fragments. On the contrary, the TDBCS calculations at 230 and 270 b initial Q_{20} both lead to similar trajectories with a global delay of $\sim$2 zs for the most compact one.

The final total kinetic energy (TKE) of the fragments is another important observable which can be used to distinguish between the fission modes. In purely adiabatic approaches, the TKE is usually estimated from the scission configuration, which is identified on the potential energy surface, based on some criteria [7,9,20]. The advantage of using the TDBCS approach is not only to include nonadiabatic effects in the formation of the fragments but also to provide a well-defined value of the TKE. Here, the TKE is computed from Coulomb and kinetic energies in postscission configurations following the method described in Ref. [19]. The resulting TKE is compared with experimental data [28] in Fig. 3. The compact symmetric mode is located near the main peak of the TKE distribution. This observation is in agreement with the experimental data, which have attributed this high TKE peak to symmetric fission [28]. The lower TKE tail is mostly attributed to the asymmetric mode. Our calculations also predict that the sef mode leads to a low TKE where only a few events have been observed experimentally.

A particularly interesting feature of quantum microscopic approaches is the possibility of investigating the role of shell effects in the dynamics. For instance, TDHF calculations have recently shown the importance of shell effects in the formation of fragments in heavy-ion collisions [35,36]. Here, shell effects in the tin region (due to the proton magic number $Z = 50$) are expected to be present in the symmetric fission mode of ^{258}Fm [28,37]. This is compatible with the spherical shape of the fragments in the scf mode (see Fig. 2) as well as with the high TKE associated with this mode. Indeed, magic fragments are difficult to excite and deform and, thus, fission occurs faster as less dissipation is involved, leading to a larger TKE. This is also compatible with the short time associated with the nonadiabatic descent of the potential to fission for the scf mode. The TDBCS calculations also confirm previous findings [19] that 60 to 80% (depending on the mode and the starting configuration) of the total excitation energy is generated during the rapid descent of the potential towards scission. This excitation energy is shared between single-particle excitation, deformation, and vibrations. A detailed analysis of this repartition will be the subject of a future work.

Another possible signature of shell effects in ^{258}Fm fission is the narrow peak in the fragment mass distribution at symmetry (see inset in Fig. 3) [30]. In order to see the influence of shell effects on the distributions, we have computed the proton number Z and neutron number N distributions in the fragments at the end of the TDBCS calculations using particle number projection techniques [27,38] with the Pfaffian calculated using an optimized algorithm [39]. The resulting distributions are shown in Fig. 5. We clearly see that the Z distribution is much sharper for the scf peak than for the other peaks, in good agreement with the expectation that this mode is dominated by spherical shell effects at $Z = 50$. The peaks in

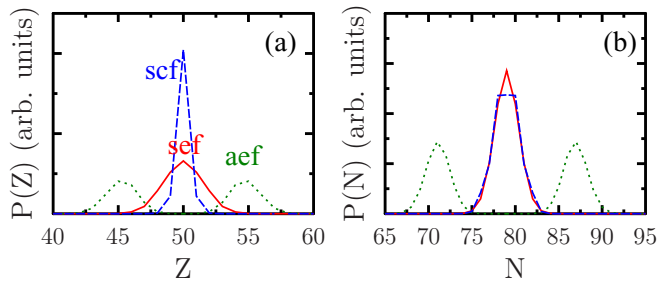

FIG. 5. (Color online) Proton (a) and neutron (b) number distributions in the fragments for the scf mode (dashed blue [gray] line), the aef mode (dotted green [gray] line), and the sef mode (solid red [gray] line).

N distributions are all of similar widths, indicating that no shell effects are contributing for neutrons. Interestingly enough, we observe a strong odd-even effect in the N distribution of the scf mode due to neutron pairing correlations, which is lower in the other modes.

It should be noted that the Z and N distributions shown in Fig. 5 are not expected to reproduce the widths of the experimental distribution for two reasons. The first reason is that these calculations account only for fluctuations acquired during the dynamical calculation. Fluctuations in the adiabatic phase are indeed expected to be important as shown, e.g., in calculations based on the time-dependent generator coordinate method [8] or using the Langevin equation [40]. The second reason is that the TDBCS approach is expected to underestimate fluctuations of one-body observables [41,42]. Yet, it would be interesting to have a better estimate of the fluctuations acquired in the dynamical phase. This can be achieved using beyond-mean-field theories such as stochastic approaches [43] or the time-dependent random-phase approximation (TDRPA) [44]. Realistic applications of the latter to nuclear dynamics have been recently achieved without pairing interaction [45–47]. Solving numerically the TDRPA equations with pairing correlations is beyond the scope of this work. Nevertheless, we have estimated the enhancement of fluctuations due to beyond-mean-field effects for the ^{264}Fm nucleus fissioning into two ^{132}Sn doubly magic nuclei in which pairing correlations can be neglected. Numerical details for solving the TDRPA equations can be found in Refs. [45–48]. As a result, the standard deviation for the distribution of the total number of nucleons A in the fragment is $\sigma_{TDRPA} = 2.35$ for the scf mode, to be compared with the TDHF result $\sigma_{TDHF} = 1.35$. This clearly indicates that beyond-mean-field fluctuations also play an important role in the dynamical phase of fission.

A fully microscopic approach to the fission process has been presented. The path to fission is divided into a slow, adiabatic evolution across the fission barrier, followed by a faster, nonadiabatic descent of the potential down to scission described with a time-dependent mean-field approach. The present approach has promising applications in various regions of the nuclear chart such as to understand the origin of the recently discovered asymmetric fission in ^{180}Hg [49] and to study neutron-rich systems of astrophysical interest for nucleosynthesis [4]. The method includes pairing correlations and can then be applied to superfluid systems across the nuclear chart. Application to the fission of ^{258}Fm shows good agreement with experimental data. In particular, this approach can be used to determine the total kinetic energy of the fragments without making any assumption on the scission configuration. Quantum shell effects are shown to play an important role in the dynamics, especially in the formation of the fragments in the dynamical phase. The method could be generalized to systems with finite temperature in order to study the disappearance of shell effects [50,51]. Beyond-mean-field fluctuations are shown to be important. Thus, a quantitative description of fragment distributions requires further developments of beyond-mean-field approaches.

We are grateful to M. Bender for his help in performing the calculations in the adiabatic phase. D. J. Hinde is thanked for useful comments and discussions. This work has been supported by the Australian Research Council Grant No. FT120100760. Part of this research was undertaken with the assistance of resources from the National Computational Infrastructure (NCI), which is supported by the Australian Government. G.S. acknowledges the Japan Society for the Promotion of Science for the JSPS postdoctoral fellowship for foreign researchers. This work was supported by Grant-in-Aid for JSPS Fellows No. 14F04769.

[1] O. Hahn and F. Strassmann, Naturwissenschaften **27**, 11 (1939).
[2] L. Meitner and O. R. Frisch, Nature (London) **143**, 239 (1939).
[3] S. G. Frauendorf and C. Guet, Ann. Rev. Nucl. Part. Sci. **51**, 219 (2001).
[4] S. Goriely, J.-L. Sida, J.-F. Lemaître, S. Panebianco, N. Dubray, S. Hilaire, A. Bauswein, and H.-T. Janka, Phys. Rev. Lett. **111**, 242502 (2013).
[5] J. Moreau and K. Heyde, in *The Nuclear Fission Process*, edited by C. Wagemans (CRC Press, Boca Raton, FL, 1991).
[6] M. Rizea and N. Carjan, Nucl. Phys. A **909**, 50 (2013).
[7] N. Dubray, H. Goutte, and J.-P. Delaroche, Phys. Rev. C **77**, 014310 (2008).
[8] H. Goutte, J. F. Berger, P. Casoli, and D. Gogny, Phys. Rev. C **71**, 024316 (2005).
[9] L. Bonneau, Phys. Rev. C **74**, 014301 (2006).
[10] A. Staszczak, A. Baran, J. Dobaczewski, and W. Nazarewicz, Phys. Rev. C **80**, 014309 (2009).
[11] J. C. Pei, W. Nazarewicz, J. A. Sheikh, and A. K. Kerman, Phys. Rev. Lett. **102**, 192501 (2009).
[12] W. Younes and D. Gogny, Phys. Rev. Lett. **107**, 132501 (2011).
[13] M. Warda and J. L. Egido, Phys. Rev. C **86**, 014322 (2012).
[14] H. Abusara, A. V. Afanasjev, and P. Ring, Phys. Rev. C **85**, 024314 (2012).
[15] M. Mirea, Phys. Lett. B **717**, 252 (2012).

[16] A. Staszczak, A. Baran, and W. Nazarewicz, Phys. Rev. C **87**, 024320 (2013).
[17] J. D. McDonnell, W. Nazarewicz, and J. A. Sheikh, Phys. Rev. C **87**, 054327 (2013).
[18] J. Sadhukhan, K. Mazurek, A. Baran, J. Dobaczewski, W. Nazarewicz, and J. A. Sheikh, Phys. Rev. C **88**, 064314 (2013).
[19] C. Simenel and A. S. Umar, Phys. Rev. C **89**, 031601 (2014).
[20] N. Schunck, D. Duke, H. Carr, and A. Knoll, Phys. Rev. C **90**, 054305 (2014).
[21] J. W. Negele, S. E. Koonin, P. Möller, J. R. Nix, and A. J. Sierk, Phys. Rev. C **17**, 1098 (1978).
[22] P. M. Goddard, P. D. Stevenson, and A. Rios, arXiv:1504.00919.
[23] B. Avez, C. Simenel, and P. Chomaz, Phys. Rev. C **78**, 044318 (2008).
[24] S. Ebata, T. Nakatsukasa, T. Inakura, K. Yoshida, Y. Hashimoto, and K. Yabana, Phys. Rev. C **82**, 034306 (2010).
[25] I. Stetcu, A. Bulgac, P. Magierski, and K. J. Roche, Phys. Rev. C **84**, 051309 (2011).
[26] Y. Hashimoto, Eur. Phys. J. A **48**, 55 (2012).
[27] G. Scamps and D. Lacroix, Phys. Rev. C **87**, 014605 (2013).
[28] E. K. Hulet, J. F. Wild, R. J. Dougan, R. W. Lougheed, J. H. Landrum, A. D. Dougan, P. A. Baisden, C. M. Henderson, R. J. Dupzyk, R. L. Hahn *et al.*, Phys. Rev. C **40**, 770 (1989).
[29] P. Möller and A. Iwamoto, Phys. Rev. C **61**, 047602 (2000).
[30] T. Ichikawa, A. Iwamoto, and P. Möller, Phys. Rev. C **79**, 014305 (2009).
[31] K.-H. Kim, T. Otsuka, and P. Bonche, J. Phys. G **23**, 1267 (1997).
[32] P. Bonche, H. Flocard, and P. H. Heenen, Comp. Phys. Com. **171**, 49 (2005).
[33] A. S. Umar and V. E. Oberacker, Phys. Rev. C **73**, 054607 (2006).
[34] J. A. Maruhn, P. G. Reinhard, P. D. Stevenson, and M. R. Strayer, Phys. Rev. C **74**, 027601 (2006).
[35] A. Wakhle, C. Simenel, D. J. Hinde, M. Dasgupta, M. Evers, D. H. Luong, R. du Rietz, and E. Williams, Phys. Rev. Lett. **113**, 182502 (2014).
[36] V. E. Oberacker, A. S. Umar, and C. Simenel, Phys. Rev. C **90**, 054605 (2014).
[37] E. K. Hulet, J. F. Wild, R. J. Dougan, R. W. Lougheed, J. H. Landrum, A. D. Dougan, M. Schadel, R. L. Hahn, P. A. Baisden, C. M. Henderson *et al.*, Phys. Rev. Lett. **56**, 313 (1986).
[38] C. Simenel, Phys. Rev. Lett. **105**, 192701 (2010).
[39] M. Wimmer, ACM Trans. Math. Softw. **38**, 30 (2012).
[40] J. Randrup and P. Möller, Phys. Rev. Lett. **106**, 132503 (2011).
[41] C. H. Dasso, T. Døssing, and H. C. Pauli, Z. Phys. A **289**, 395 (1979).
[42] R. Balian and M. Véneroni, Phys. Rev. Lett. **47**, 1353 (1981).
[43] D. Lacroix and S. Ayik, Eur. Phys. J. A **50**, 95 (2014).
[44] R. Balian and M. Véneroni, Phys. Lett. B **136**, 301 (1984).
[45] J. M. A. Broomfield and P. D. Stevenson, J. Phys. G **35**, 095102 (2008).
[46] C. Simenel, Phys. Rev. Lett. **106**, 112502 (2011).
[47] C. Simenel, Eur. Phys. J. A **48**, 152 (2012).
[48] P. Bonche and H. Flocard, Nucl. Phys. A **437**, 189 (1985).
[49] A. N. Andreyev, J. Elseviers, M. Huyse, P. Van Duppen, S. Antalic, A. Barzakh, N. Bree, T. E. Cocolios, V. F. Comas, J. Diriken *et al.*, Phys. Rev. Lett. **105**, 252502 (2010).
[50] J. D. McDonnell, W. Nazarewicz, J. A. Sheikh, A. Staszczak, and M. Warda, Phys. Rev. C **90**, 021302 (2014).
[51] N. Schunck, D. Duke, and H. Carr, Phys. Rev. C **91**, 034327 (2015).